Available online at www.sciencedirect.com
SCIENCE DIRECT®
International Journal of Solids and Structures 42 (2005) 2489–2504
INTERNATIONAL JOURNAL OF SOLIDS and STRUCTURES
www.elsevier.com/locate/ijsolstr

Micromechanics of fabric reinforced composites with periodic microstructure

Ever J. Barbero [a,*], Thomas M. Damiani [a], Jonathan Trovillion [b]

[a] *Department of Mechanical and Aerospace Engineering, West Virginia University, 323 ESB, Morgantown, WV 26506-6106, United States*
[b] *Construction Engineering Research Laboratory, US Army Corps of Engineers, Champaign, IL 61822-1076, United States*

Received 19 September 2004
Available online 2 November 2004

Abstract

A model to predict the effective stiffness of woven fabric composite materials is presented. Taking advantage of the inherent periodicity of woven fabric architecture, periodic microstructure theory is used at the mesoscale for the case of a two-phase heterogeneous material with multiple periodic inclusions. For plain weave fabrics, the representative volume element (RVE) is discretized into fiber/matrix bundles and the pure matrix regions that surround them. The surfaces of the fiber/matrix bundles are fit with sinusoidal equations using two approaches. The first is based on measurements taken from photomicrographs of composite specimens and the second is based on an idealized representation of the plain weave structure. Three-dimensional sinusoidal surfaces are generated from the face equations and weave shape for the real and idealized cases in order to mathematically describe the fiber/matrix bundle regions, which are treated as unidirectional composites. Model results from the idealized geometry are compared to experimental data from the literature and show good agreement, including interlaminar material properties. From a comparison of the real and idealized geometry results for similar material RVE dimensions, it is seen that the model is capable of predicting significant changes in the in-plane material properties from slight mismatch in the fiber/matrix bundle shape and crimp, which can be captured using the geometric surfaces generated from photomicrograph measurements.

1. Background

An increasing number of fiber reinforced composite components are being fabricated with load-carrying fibers, which are woven to form a fabric. This reinforcement system has advantages with respect to

* Corresponding author. Tel.: +304 2933 111; fax: +304 2936 689.
E-mail address: ebarbero@wvu.edu (E.J. Barbero).

0020-7683/$ - see front matter © 2004 Published by Elsevier Ltd.
doi:10.1016/j.ijsolstr.2004.09.034

fabrication as well as mechanical properties. The weaving and interlacing of the fiber tows produces a self-supporting system that can be draped and manipulated to form complex shapes. Mechanically, the geometry of a fabric provides bi-directional stiffness in the plane of loading (E_1, E_2), increased interlaminar stiffness out of the plane of loading (E_3, G_{13}, G_{23}), and superior impact tolerance. For this class of fiber-reinforced composite, the prediction of an effective set of material properties is significantly more complex than for unidirectional ply laminates. The complexity is due to the weaving and interlacing of the fiber tows. The objective of this research is to develop an analytical model that predicts a complete set of orthotropic effective material properties for woven fabric composites based solely on the properties of the constituent materials.

Significant research pertaining to the modeling of woven fabric composites has been conducted over the past 20 years. Most of the analytical models initially developed are based on classical lamination theory (CLT). Using CLT, the representative volume element (RVE) is idealized as a series of cross-ply laminates that are stacked in a sequence that resembles the woven fabric architecture (Fig. 1), while the geometry used in this work is depicted in Fig. 2. CLT was first used in the mosaic, fiber undulation, and bridging models (Ishikawa and Chou, 1982). Subsequent research further extended CLT using more complex discretization schemes and iterative approaches (Hahn and Pandey, 1994; Ito and Chou, 1998; Ito and Chou, 1997; Naik and Ganesh, 1996; Aboudi, 1991; Scida et al., 1999; Vandeurzen et al., 1996a; Vandeurzen et al., 1996b). CLT is relatively easy to implement and predicts well the longitudinal moduli for plain weave fabric composite. Since these models neglect or roughly approximate the actual undulated woven geometry, they are

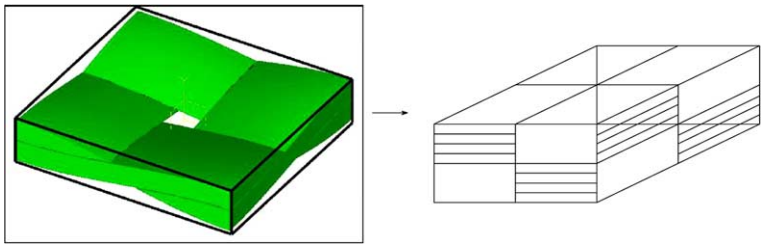

Fig. 1. CLT idealization of a plain weave fabric RVE (showing 1/2 the period in the in-plane directions).

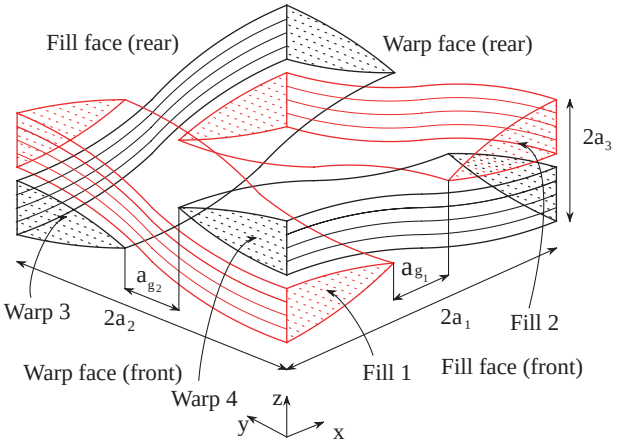

Fig. 2. Mesoscale analysis of a plain weave fabric RVE (1/2 period shown in-plane (x-y)).

ineffective at calculating the out-of-plane and shear moduli. Other methods of predicting plain weave fabric composite material properties include the energy equivalence method (Zhang and Harding, 1990), variational potential energy (Zhong and Van Hoa, 2001), and full-scale discretization using the finite element method (Dasgupta et al., 1996; Dasgupta and Bhandarkar, 1994; Kollegal and Sridharan, 2000a; Kollegal and Sridharan, 2000b; Kollegal and Sridharan, 1998; Sheng and Hoa, 2001; Kuhn and Charalambides, 1998a; Kuhn and Charalambides, 1998b; Aitharaju and Averill, 1999; Kuhn and Charalambides, 1999; Blackketter et al., 1993). These methods are significantly more powerful and comprehensive than CLT, but are also much more complicated and computationally expensive to implement.

The concept of exploiting geometric periodicity through the technique of periodic microstructure is widely known and accepted. This technique was originally developed to analyze materials with periodically distributed micro cracks or micro voids (Nemat-Nasser and Hori, 1993). A micromechanical model to predict particulate composite material properties was developed in (Nemat-Nasser et al., 1993). The author has also developed a micromechanical model for unidirectional fiber reinforced ply lamina material properties through an assumed periodic distribution of fiber reinforcement (Luciano and Barbero, 1994; Barbero and Luciano, 1995). The objective of this research is to use the existing periodic microstructure theory applied at the meso-level to model the undulating fiber/matrix tows as periodic inclusions, and then modify the analytical scheme for prediction of the overall material properties of a plain weave fabric reinforced composite material. A brief overview of the existing theory and modifications necessary for modeling fiber/matrix tow regions at the mesoscale are presented.

2. Periodic microstructure

Periodic microstructure mechanics exploits the geometric periodicity of the system in order simplify the mechanical field variables, such as the stress, strain, and stiffness. In general, all of these terms are functions of position inside of the representative volume element (RVE). The periodicity of a plain weave fabric RVE enables expansion of the field variables in terms of a three dimensional Fourier series, thus creating more simplified and workable expressions. The expansion is generally expressed as

$$\underline{\varepsilon}(\underline{x}) = \sum_{\xi}{}' [F\underline{\varepsilon}(\underline{\xi}) \cdot \exp(\mathrm{i}\underline{x} \cdot \underline{\xi})] \tag{1}$$

in which the Fourier coefficients are

$$F\underline{\varepsilon}(\underline{\xi}) = \frac{1}{U} \int_U \underline{\varepsilon}(\underline{x}) \cdot \exp(-\mathrm{i}\underline{x} \cdot \underline{\xi}) \mathrm{d}V \tag{2}$$

$$\underline{\xi} = \xi_i = \xi_i(n_i) = \frac{n_i \pi}{a_i} \tag{3}$$

and a_i is 1/2 the length of each RVE dimension. The number of terms N in the Fourier expansion influences the accuracy of the Fourier series in representing the field variable. All of the possible combinations of n_1, n_2, and n_3 ranging from $-N$ to N, with the exclusion of the term when the n values are all equal to zero, are employed in the expansion of all relevant field variables (Luciano and Barbero, 1994; Barbero and Luciano, 1995).

Periodic microstructure has already been used successfully to predict the material properties of fiber reinforced unidirectional ply lamina in (Luciano and Barbero, 1994; Barbero and Luciano, 1995). In order to apply this technique to a plain weave fabric RVE, the in situ impregnated fiber tows are assumed to be transversely isotropic inclusions in the RVE surrounded by un-reinforced matrix pockets. These inclusions consist of unidirectional composite reinforced with fiber bundles. The fibers in the inclusions undulate in a sinusoidal pattern, as seen in Fig. 2.

3. Homogenization using an eigenstrain

Use of periodic microstructure enables the expression of field variables, which are generally functions of position, in a workable manner. The material is heterogeneous, with two distinct material regions: the inclusions and the matrix that surrounds the inclusions. The inclusions are transversely isotropic. The surrounding matrix is isotropic. In order to obtain a single set of effective material properties, these two regions are homogenized into a region with a single set of material properties. Since the matrix is a much simpler material to represent, the inclusions Ω are homogenized to the surrounding matrix material M using an eigenstrain (Nemat-Nasser and Hori, 1993). The stiffness matrix C^{Ω} of the fiber tow inclusions are homogenized to the stiffness C of the surrounding matrix through the calculation of the eigenstrain, which is a corrective strain term added to satisfy the consistency condition. The homogenization scheme, which is expressed in terms of a uniformly applied macrostrain ε^{o} to the system, is expressed as

$$\underline{\sigma}(\underline{x}) = \underline{\underline{C}} : \left(\underline{\varepsilon}^{o} + \underline{\varepsilon}^{P}(\underline{x})\right) \quad \text{in } M \tag{4}$$

$$\underline{\sigma}(\underline{x}) = \underline{\underline{C}}^{\Omega} : \left(\underline{\varepsilon}^{o} + \underline{\varepsilon}^{P}(\underline{x})\right) \quad \text{in } \Omega \tag{5}$$

Eqs. (4) and (5) represent the constitutive equations for regions surrounding the inclusions M and inside of the inclusion Ω, respectively. The concept of homogenization in the context of multi-phase composite materials was initially developed by Mori and Tanaka (1973) and further modified by Weng (1984) for application to particulate composites. The periodic disturbance strain, denoted ε^{P}, is the strain produced due to the presence of the inclusions. This term is written through a Fourier expansion as

$$\underline{\varepsilon}^{P}(\underline{x}) = \sum_{\underline{\xi}}{}' F\underline{\underline{S}}^{P}(\underline{\xi}) : \left[\frac{1}{U}\int_{U} \underline{\varepsilon}^{*}(\underline{y}) \cdot \exp(i\underline{\xi} \cdot (\underline{x} - \underline{y}))\, dV_{y}\right] \tag{6}$$

in which the term FS^{P} is the Fourier coefficient of the periodic integral operator, which relates the periodic disturbance strain to the eigenstrain. The homogenization of a general heterogeneous RVE modifies Eq. (5) to the following form

$$\underline{\sigma}(\underline{x}) = \underline{\underline{C}} : \left(\underline{\varepsilon}^{o} + \underline{\varepsilon}^{P}(\underline{x}) - \underline{\varepsilon}^{*}(\underline{x})\right) = \left\{ \begin{array}{ll} \underline{\underline{C}} : (\underline{\varepsilon}^{o} + \underline{\varepsilon}^{P}(\underline{x})) & \text{in } M \\ \underline{\underline{C}} : (\underline{\varepsilon}^{o} + \underline{\varepsilon}^{P}(\underline{x}) - \underline{\varepsilon}^{*}(\underline{x})) & \text{in } \Omega \end{array} \right\} \tag{7}$$

in which the stiffness of the inclusion, C^{Ω}, is replaced by the stiffness of the surrounding matrix, C and the term $\varepsilon^{*}(x)$ is the eigenstrain, a corrective term added to the constitutive equation to balance out the modified stiffness term. The process of homogenization is valid only if the resulting stress at a given position remains unchanged by the correction. This restriction is referred to as the consistency condition and is written as

$$\underline{\underline{C}}^{\Omega}(\underline{x}) : (\varepsilon^{o} + \varepsilon^{P}(\underline{x})) = \underline{\underline{C}} : \left(\varepsilon^{o} + \varepsilon^{P}(\underline{x}) - \varepsilon^{*}(\underline{x})\right) \tag{8}$$

The eigenstrain is a function of position and bounded by the dimensions of the inclusions. Through the use of Fourier expansion and eigenstrain homogenization, the effective material properties of a plain weave fabric composite can be determined.

4. Average Eigenstrain approximation

Through expansion and simplification of all terms in Eq. (8) that are functions of position (Damiani, 2003), the consistency condition is written by Nemat-Nasser and Hori (1993) as

$$F\underline{\underline{C}}^{\Omega}(\underline{\xi}):\underline{\varepsilon}^{o}+\left[\sum_{\zeta}{}'F\underline{\underline{C}}^{\Omega}(\underline{\xi}-\underline{\zeta}):F\underline{\underline{S}}^{P}(\underline{\zeta}):F\underline{\varepsilon}^{*}(\underline{\zeta})\right]=\underline{\underline{C}}:\left[\underline{\varepsilon}^{o}+F\underline{\underline{S}}^{P}(\underline{\xi}):F\underline{\varepsilon}^{*}(\underline{\xi})-F\underline{\varepsilon}^{*}(\underline{\xi})\right] \tag{9}$$

in which FC^{Ω}, FS^{P}, $F\varepsilon^{*}$ are the Fourier coefficients of the inclusion stiffness, periodic integral operator (relating the disturbance strain ε^{P} to the eigenstrain ε^{*}), and the periodic eigenstrain, respectively. These terms are summarized as follows:

$$F\underline{\underline{C}}^{\Omega}(\underline{\xi})=\frac{1}{U}\int_{U}\underline{\underline{C}}^{\Omega}(\underline{x})\cdot\exp(-\mathrm{i}\underline{x}\cdot\underline{\xi})\,\mathrm{d}V \tag{10}$$

$$F\underline{\underline{S}}^{P}(\underline{\xi})=\mathrm{sym}\left[\underline{\xi}\otimes(\underline{\xi}\cdot\underline{\underline{C}}\cdot\underline{\xi})^{-1}\otimes\underline{\xi}\right]:\underline{\underline{C}} \tag{11}$$

$$F\underline{\varepsilon}^{*}(\underline{\xi})=\frac{1}{U}\int_{U}\underline{\varepsilon}^{*}(\underline{x})\cdot\exp(-\mathrm{i}\underline{x}\cdot\underline{\xi})\,\mathrm{d}V \tag{12}$$

The significance of Eq. (9) is that all of the original field variables in Eq. (8) have been replaced by Fourier coefficient terms. Eq. (9) represents a linear system of equations over the number of ξ terms taken, the solution of which is the Fourier coefficient of the eigenstrain, $F\varepsilon^{*}$.

In order to determine the effective stiffness matrix for a plain weave fabric composite, it is assumed that the eigenstrain is a constant value, denoted $\overline{\varepsilon}^{*}$. For a heterogeneous RVE with multiple inclusions Eq. (8) becomes (Nemat-Nasser and Hori, 1993)

$$\left(\underline{\underline{C}}^{\Omega}\right)^{\alpha}:\left(\varepsilon^{o}+\sum_{\beta=1}^{n}S^{P}(\Omega_{\alpha},\Omega_{\beta}):\overline{\varepsilon}^{*\beta}\right)=\underline{\underline{C}}:\left(\varepsilon^{o}+\sum_{\beta=1}^{n}\left[S^{P}(\Omega_{\alpha},\Omega_{\beta})-\delta_{\alpha\beta}I^{(4s)}\right]:\overline{\varepsilon}^{*\beta}\right) \tag{13}$$

where α and β represent indexes over the number of inclusions. Eq. (13) is the periodic consistency condition for multiple inclusions and an average eigenstrain approximation. The periodic integral operator for this case, as is the case with a plain weave fabric, is

$$S^{P}(\Omega_{\alpha},\Omega_{\beta})=\sum_{\xi}{}'f_{\alpha}\cdot g_{\alpha}(-\underline{\xi})g_{\beta}(\underline{\xi})FS^{P}(\underline{\xi}) \tag{14}$$

in which the g-integral terms are expressed as

$$g_{\alpha}(\underline{\xi})=\frac{1}{\Omega_{\alpha}}\int_{\Omega_{\alpha}}\exp(\mathrm{i}\underline{\xi}\cdot\underline{x})\,\mathrm{d}V \tag{15}$$

The periodic integral operator, S^{P}, takes into account the interaction between the various inclusions inside of an RVE. For the plain weave fabric case, α and β are numbered indexes from 1 to 4. Thus, S^{P} results in a $6*m$ by $6*m$ matrix in which m is the number of inclusions inside of the RVE. Finally, in this work we propose that the effective stiffness for multiple inclusions can be expressed as

$$\overline{\underline{\underline{C}}}=\underline{\underline{C}}:\left\{I^{(4s)}-\sum_{\alpha=1}^{m}f_{\alpha}\left[\sum_{\beta=1}^{m}A_{\alpha\beta}^{-1}:\left(\underline{\underline{C}}^{\alpha}-\underline{\underline{C}}\right):I^{(4s)}\right]\right\} \tag{16}$$

where

$$\underline{\underline{A}}=\underline{\underline{C}}:\left(\underline{\underline{S}}^{P}(\Omega_{\alpha},\Omega_{\beta})-\delta_{\alpha\beta}I^{(4s)}\right)-\underline{\underline{C}}^{\Omega^{\alpha}}:\underline{\underline{S}}^{P}(\Omega_{\alpha},\Omega_{\beta}) \tag{17}$$

in which $\delta_{\alpha\beta}$ is the Dirac delta function and $C^{\Omega^{*}}$ is the averaged mesoscale stiffness of a given inclusion. Eq. (16) represents the effective stiffness of a two-phase heterogeneous material with m inclusions of stiffness $C^{\Omega^{*}}$

surrounded by an isotropic material of stiffness C. A plain weave fabric composite can be analyzed in this manner if the fiber/matrix tows are treated as the inclusions surrounded by pure matrix regions.

5. Geometric characterization of the inclusions

Determination of the effective material properties for a plain-weave fabric using periodic microstructure and homogenization requires the bounds (surfaces) of the fiber/matrix inclusions to be known so that the integration in Eq. (15) can be performed. The Construction Engineering Research Laboratory (CERL) of the US Army Corps of Engineers captured detailed photomicrographs of the four faces inherent in a cuboid RVE for an AS4/vinylester plain weave fabric. In addition, Ito and Chou (1998) developed analytical expressions for a geometric description of the inclusion bounds based on RVE and tow dimensions. The distinction between the two approaches is that the Ito and Chou representation is idealized, resulting in identical weave patterns in the warp and fill directions, along with constant inclusion thicknesses. The photomicrographs from CERL are measured and averaged over several RVE's. There is slight mismatch between the warp and fill faces of the CERL geometry (Fig. 2), resulting in the warp and fill tows having different thicknesses and degrees of tow crimp. The effects of such a mismatch on material property characterization will be discussed in Section 7. Once the inclusion geometry has been completely described, the equations derived in Section 4 can be evaluated and the effective material properties of the RVE can be determined.

In addition to the CERL geometry, the geometric parameters of the following plain weave laminae are used to generate inclusion surface bounds: AS4 carbon/vinylester fabric (Ito and Chou, 1998), E-glass/vinylester fabric (Scida et al., 1999), E-glass/epoxy fabric (Kollegal and Sridharan, 2000b), and T300/epoxy (Sheng and Hoa, 2001). For each case, the RVE and tow parameters are used as inputs into the idealized face equations. The dimensions of the RVE geometries are listed in Table 1 and depicted in Fig. 2. The volume of the RVE is $8(a_1)(a_2)(a_3)$ and a_g is the smallest distance between adjacent inclusions.

5.1. Mapping the two dimensional faces of the RVE

A typical photomicrograph of the CERL geometry is shown in Fig. 3. It reveals the cross-sectional bounds of the inclusions running out of the plane, as well as the undulating shape of the inclusions in the plane. From photomicrographs of the RVE faces, the bounds of the out-of-plane cross-section and in-plane weave shape for the warp and fill inclusions are digitized using the program GRABIT, a simple excel macro used to transcribe pictures into graphs. The series of data points are then fit to a sinusoidal function of the form

$$f(x) = A\sin(B\cdot x + C) + D \tag{18}$$

In this research, A and D have units of meters (m), B has units of inverse meters (1/m), and C is dimensionless. For each face of the CERL geometry, four sinusoidal curves of the form of Eq. (18) are generated from the photomicrographs. The curve fit parameters of the CERL geometry follow the form of Eq. (18). For example, the front fill face (see Fig. 2) is represented by the following equations:

$$\mathrm{top}_{\mathrm{f1f}}(x) = .000129\cdot\sin[-2153\cdot x - 0.41] + .000091 \tag{19}$$

$$\mathrm{bot}_{\mathrm{f1f}}(x) = .0000744\cdot\sin[1710\cdot x] + .000106 \tag{20}$$

$$\mathrm{top}_{\mathrm{f2f}}(x) = .0000744\cdot\sin[1710\cdot x] - .000106 \tag{21}$$

$$\mathrm{bot}_{\mathrm{f2f}}(x) = -.000161\cdot\sin[-1874\cdot x + 9.59] - .0000585 \tag{22}$$

where the subscript f1f denotes fill 1 front face. Note that Eqs. (20) and (21) define the bottom cross-section bound of fill 1 and the top bound of fill 2, and both equations represent the undulating shape of warp 4 as

Table 1
Dimension parameters and material property data for the fabric geometries (moduli in GPa)

	CERL geometry	Idealized geometry			
		Ito and Chou (1998)	Scida et al. (1999)	Kollegal and Sridharan (2000b)	Sheng and Hoa (2001)
Fiber	Carbon AS4-D	Carbon AS4-D	E-glass	E-glass	Carbon T300
E_f	221	221	72.3	72.3	230
v_f	0.22	0.22	0.26	0.26	0.26
Matrix	Vinylester	Vinylester	Vinylester	Epoxy	Epoxy
E_m	3.4	3.4	3.4	3.12	3.12
v_m	0.35	0.35	0.35	0.38	0.38
Tow data	All tow properties found using isotropic periodic microstructure micromechanics (Luciano and Barbero, 1994)				
$V_{f,tow}$	0.724[a]	0.735[b] (0.42)	0.798[c]	0.697[c]	0.752[b] (0.44)
E_1	160.755	163.302	58.397	51.352	173.864
E_2	19.489	20.252	20.865	15.04	22.135
v_{12}	0.28	0.279	0.241	0.262	0.278
v_{23}	0.415	0.417	0.386	0.437	0.42
G_{12}	7.393	7.757	8.465	5.342	8.611
G_{23}	6.886	7.147	7.527	5.232	7.796
RVE geometry parameters					
a_1 (μm)	920	1608	600	310	480
a_2 (μm)	920	1528	600	310	550
a_3 (μm)	250	318	50	100	80
a_{g1} (μm)	170	317	20	20	151
a_{g2} (μm)	170	275	20	20	11

[a] Estimated from overall fiber volume fraction of idealized CERL geometry, see Section 7.
[b] Calculated according to Eq. (44) in Section 7.
[c] Data from references.

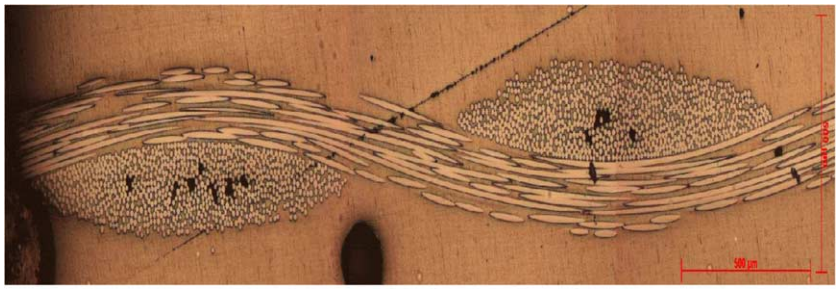

Fig. 3. Rear warp face of the fabric geometry of CERL.

shown in Fig. 4. For the idealized geometry, the fitting parameters are represented as a function of the RVE geometric dimensions (see Fig. 2). The idealized cross-section bounds for a generic front fill face are represented as

$$\mathrm{top}_{\mathrm{f1fi}}(x) = \left[-\frac{a_3}{2}\cdot\sin\left(\frac{\pi\cdot a_{g_1}}{4\cdot a_1}\right)-\frac{a_3}{2}\right]\cdot\sin\left[\frac{\pi}{(a_{g_1}-2\cdot a_1)}\cdot x-\frac{\pi\cdot(a_{g_1}-4\cdot a_1)}{2\cdot(a_{g_1}-2\cdot a_1)}\right] - \frac{a_3}{2}\cdot\sin\left(\frac{\pi\cdot a_{g_1}}{4\cdot a_1}\right)+\frac{a_3}{2} \tag{23}$$

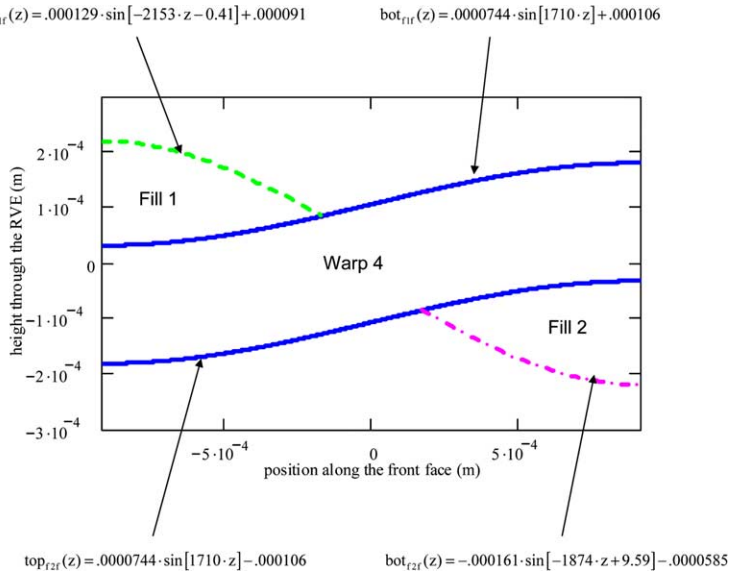

Fig. 4. Front fill face plot of the CERL geometry with face equations found through photomicrographs (1/2 period shown).

$$\mathrm{bot}_{\mathrm{f1fi}}(x) = \frac{a_3}{2}\sin\left(\frac{\pi}{2\cdot a_1}\cdot x\right) + \frac{a_3}{2} \tag{24}$$

$$\mathrm{top}_{\mathrm{f2fi}}(x) = \frac{a_3}{2}\sin\left(\frac{\pi}{2\cdot a_1}\cdot x\right) + \frac{a_3}{2} \tag{25}$$

$$\mathrm{bot}_{\mathrm{f2fi}}(x) = \left[-\frac{a_3}{2}\cdot\sin\left(\frac{\pi\cdot a_{g_1}}{4\cdot a_1}\right) - \frac{a_3}{2}\right]\cdot\sin\left[\frac{\pi}{(a_{g_1}-2\cdot a_1)}\cdot x + \frac{\pi\cdot(a_{g_1}-4\cdot a_1)}{2\cdot(a_{g_1}-2\cdot a_1)}\right] + \frac{a_3}{2}\cdot\sin\left(\frac{\pi\cdot a_{g_1}}{4\cdot a_1}\right) - \frac{a_3}{2} \tag{26}$$

where the subscript f1fi denotes fill 1 front face idealized. For each plain weave geometry used in the analysis, there is a set of equations defining the cross-sectional bound and undulating shape of each tow. The curve fitting parameters are listed in Table 2 for each face of the respective RVE.

5.2. Generation of surface functions from the face boundaries

From the two-dimensional plots created in Section 5.1, two things can be determined for a given cross-section: (a) the shape of the inclusion cross-section on each face of the RVE and (b) the undulation of each inclusion. The three-dimensional surface function bounds are determined by a three-dimensional curve fit in which the curves defined on the respective RVE faces are the conditions or boundaries used to determine the surface parameters, which are similar to the curve fitting parameters of Section 5.1 but are now functions instead of constants. The fill inclusions (1 and 2 in Fig. 2) normal to the x-direction and extending in the y-direction are fit to sinusoidal surface functions of the form

$$F_0(x,y) = A(x)\cdot\sin(B(x)\cdot y + C(x)) + D(x) \tag{27}$$

Table 2
Curve fit parameters of RVE faces for various fabric geometries Eq. (18)

	Fill 1 front face		Fill 1 rear face		Fill 2 front face		Fill 2 rear face		Warp 3 front face		Warp 3 rear face		Warp 4 front face		Warp 4 rear face	
	Top	Bottom	Top	Bottom	Top	Bottom	Top	Bottom	Top	Bottom	Top	Bottom	Top	Bottom	Top	Bottom
CERL																
A (m)	1.29E−4	7.44E−5	7.44E−5	−2.01E−4	7.44E−5	−1.61E−4	1.04E−4	7.44E−5	1.26E−4	1.38E−4	1.38E−4	−2.25E−4	1.38E−4	9.37E−5	−1.89E−4	1.38E−4
B (1/m)	−2153.1	1710	1710	1646	1710	−1874	2499	1710	1980	1727	1727	1416	1727	2406	1561	1727
C	−0.4100	0	π	3.09	0	9.59	−0.729	π	−0.251	π	0	0.269	π	0.642	−0.134	0
D (m)	9.10E−5	1.06E−4	−1.06E−4	−1.9E−5	−1.06E−4	−5.85E−5	1.16E−4	1.06E−4	4.31E−5	9.38E−5	−9.38E−5	5.55E−5	−9.38E−5	−7.59E−5	−1.93E−5	9.38E−5
Ito and Chou (1998)																
A (m)	−1.89E−4	1.59E−4	−1.59E−4	1.89E−4	1.59E−4	−1.89E−4	1.89E−4	−1.59E−4	1.81E−4	1.59E−4	1.59E−4	−1.81E−4	−1.59E−4	1.81E−4	−1.81E−4	1.59E−4
B (1/m)	−1112	977	977	−1112	977	−1112	−1112	977	−1130	1028	1028	−1130	1028	−1130	−1130	1028
C	−3.36	0	0	−3.36	0	3.36	3.36	0	3.30	0	0	3.30	0	−3.30	−3.30	0
D (m)	1.29E−4	1.59E−4	−1.59E−4	−1.29E−4	−1.59E−4	−1.29E−4	1.29E−4	1.59E−4	1.37E−4	1.59E−4	−1.59E−4	−1.37E−4	1.59E−4	−1.37E−4	1.37E−4	1.59E−4
Scida et al. (1999)																
A (m)	−2.57E−4	2.5E−5	−2.5E−5	2.57E−5	2.5E−5	−2.57E−5	2.57E−5	−2.5E−5	2.57E−5	2.5E−5	2.5E−5	−2.57E−5	−2.5E−5	2.57E−5	−2.57E−5	2.5E−5
B (1/m)	−2662	2618	2618	−2662	2618	−2662	−2992	2618	−2662	2618	2618	−2992	2618	−2662	−2662	2618
C	−3.17	0	0	−3.17	0	3.17	3.17	0	3.17	0	0	3.17	0	−3.17	−3.17	0
D (m)	2.43E−5	2.5E−5	−2.5E−5	−2.43E−5	−2.5E−5	−2.43E−5	2.43E−5	2.5E−5	2.43E−5	2.5E−5	−2.5E−5	−2.43E−5	2.5E−5	−2.43E−5	2.43E−5	2.5E−5
Kollegal and Sridharan (2000b)																
A (m)	−5.25E−5	5.00E−5	−5.00E−5	5.25E−5	5.00E−5	−5.25E−5	5.25E−5	−5.00E−5	5.25E−5	5.00E−5	5.00E−5	−5.25E−5	−5.00E−5	5.25E−5	−5.25E−5	5.00E−5
B (1/m)	−5236	5067	5067	−5236	5067	−5236	−5236	5067	−5236	5067	5067	−5236	5067	−5236	−5236	5067
C	−3.19	0	0	−3.19	0	3.19	3.19	0	3.19	0	0	3.19	0	−3.19	−3.19	0
D (m)	4.75E−5	5.00E−5	−5.00E−5	−4.75E−5	−5.00E−5	−4.75E−5	4.75E−5	5.00E−5	4.75E−5	5.00E−5	−5.00E−5	−4.75E−5	5.00E−5	−4.75E−5	4.75E−5	5.00E−5
Sheng and Hoa (2001)																
A (m)	−4.98E−5	4.00E−5	−4.00E−5	4.98E−5	4.00E−5	−4.98E−5	4.98E−5	−4.00E−5	4.06E−5	4.00E−5	4.00E−5	−4.06E−5	−4.00E−5	4.06E−5	−4.06E−5	4.00E−5
B (1/m)	−3883	3272	3272	−3883	3272	−3883	−3883	3272	−2884	2856	2856	−2884	2856	−2884	−2884	2856
C	−3.43	0	0	−3.43	0	3.43	3.43	0	3.16	0	0	3.19	0	−3.16	−3.16	0
D (m)	3.02E−5	4.00E−5	−4.00E−5	−3.02E−5	−4.00E−5	−3.02E−5	3.02E−5	4.00E−5	3.94E−5	4.00E−5	−4.00E−5	−3.94E−5	4.00E−5	−3.94E−5	3.94E−5	4.00E−5

The warp inclusions (3 and 4 in Fig. 2) normal to the y-direction and extending in the x-direction are fit with

$$F_{90}(x,y) = A(y)\cdot\sin(B(y)\cdot x + C(y)) + D(y) \tag{28}$$

The front and rear faces of the RVE yield the upper and lower cross-section bounds for each inclusion. For Fill 1, the lower bound of the fill cross-section on the front face is taken as the upper bound of Warp 4 (see Figs. 2 and 5). The opposite is the case on the rear face in which the upper bound of Fill 1 on the rear face is the lower bound of Warp 3. The equations that bound these faces are of the form of Eq. (18), and the A, B, C, and D parameters are given in Table 2 and subsequently plotted for the front fill face in Fig. 4. From the complete description of each face of the RVE, two conditions are extracted for creating each surface function. The other two conditions are generated by assuming that the slope of the undulation with respect to the fiber direction is equal to zero at the front and rear faces, respectively. Then the four parameters described by $A(x)$, $B(x)$, $C(x)$, and $D(x)$ in Eqs. (27) and (28) can be determined from the face equations and the slope constraints. Each inclusion is represented by two surface functions bounding the upper and lower portions of the fiber/matrix bundles. For a plain weave fabric, a total of eight surface functions are generated that completely define the four inclusions of the RVE. For the CERL geometry, the top bound of the Fill 1 inclusion is represented as

$$A_{\mathrm{Tf1}}(x) = -.0000372\cdot\sin(1710\cdot x) - .0000988 + .0000645\cdot\sin(2150\cdot x + .41) \tag{29}$$

$$B_{\mathrm{Tf1}}(x) = 1710 \tag{30}$$

$$C_{\mathrm{Tf1}}(x) = 0 \tag{31}$$

$$D_{\mathrm{Tf1}}(x) = -.0000372\cdot\sin(1710\cdot x) - .00000726 - .0000645\cdot\sin(2150\cdot x + .41) \tag{32}$$

$$\mathrm{top}_{\mathrm{f1}}(x,y) = A_{\mathrm{Tf1}}(x)\cdot\sin(B_{\mathrm{Tf1}}(x)\cdot y + C_{\mathrm{Tf1}}(x)) + D_{\mathrm{Tf1}}(x) \tag{33}$$

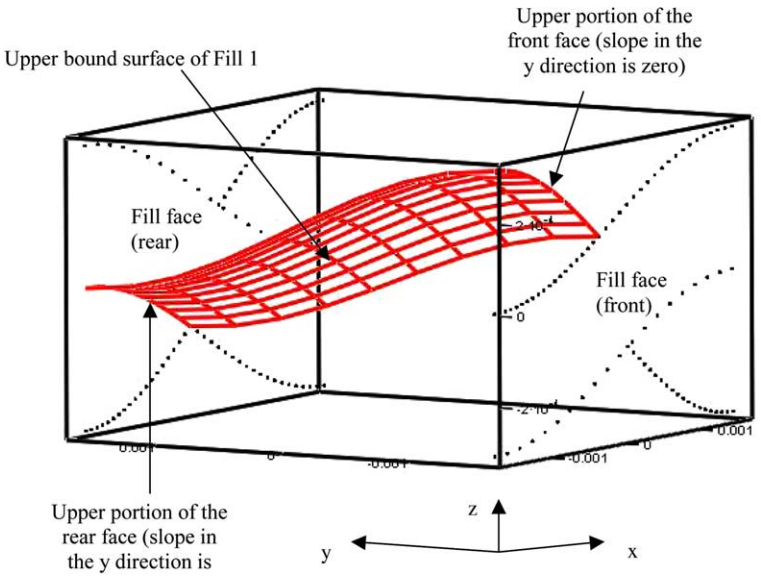

Fig. 5. Illustration of three-dimensional surface function mapping for the upper bound of fill 1 in the CERL geometry (1/2 period shown).

An illustration is shown in Fig. 5. For the idealized geometry, the surface that describes the top bound of Fill 1 is represented as

$$A_{\mathrm{Tf1i}}(x) = -\frac{a_3}{4}\sin\left(\frac{\pi x}{2a_1}\right) - \frac{a_3}{2} + \frac{a_3}{4}\sin\left[\frac{\pi(2x - a_{g_1} + 4a_1)}{2(a_{g_1} - 2a_1)}\right]\sin\left(\frac{\pi a_{g_1}}{4a_1}\right) + \frac{a_3}{4}\sin\left[\frac{\pi(2x - a_{g_1} + 4a_1)}{2(a_{g_1} - 2a_1)}\right] + \frac{a_3}{4}\sin\left(\frac{\pi a_{g_1}}{4a_1}\right) \tag{34}$$

$$B_{\mathrm{Tf1i}}(x) = \frac{\pi}{2a_2} \tag{35}$$

$$C_{\mathrm{Tf1i}}(x) = 0 \tag{36}$$

$$D_{\mathrm{Tf1i}}(x) = -\frac{a_3}{4}\sin\left(\frac{\pi x}{2a_1}\right) - \frac{a_3}{4}\sin\left[\frac{\pi(2x - a_{g_1} + 4a_1)}{2(a_{g_1} - 2a_1)}\right]\sin\left(\frac{\pi a_{g_1}}{4a_1}\right) - \frac{a_3}{4}\sin\left[\frac{\pi(2x - a_{g_1} + 4a_1)}{2(a_{g_1} - 2a_1)}\right] - \frac{a_3}{4}\sin\left(\frac{\pi a_{g_1}}{4a_1}\right) \tag{37}$$

$$\mathrm{top}_{\mathrm{f1i}}(x, y) = A_{\mathrm{Tf1i}}(x) \cdot \sin(B_{\mathrm{Tf1i}}(x) \cdot y + C_{\mathrm{Tf1i}}(x)) + D_{\mathrm{Tf1i}}(x) \tag{38}$$

The graphic representation for the surfaces bounding the entire plain weave fabric is seen in Fig. 6 for the CERL geometry.

Generating surface functions for each inclusion bound is necessary for implementing the periodic microstructure model. The inclusion bounds can now be used to compute volume fractions for each inclusion to the entire RVE, as well as various terms necessary to solving the effective stiffness (Eqs. (11), (14), (15), (17)).

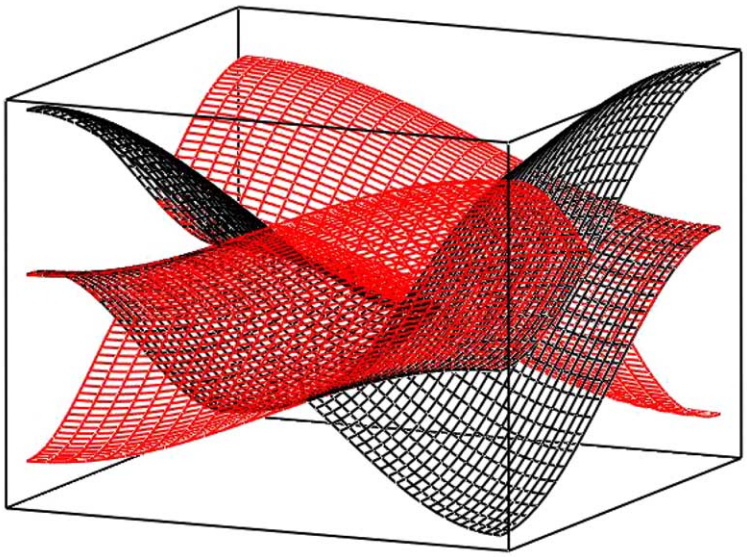

Fig. 6. Plot of the surface bounds for the inclusions of a plain weave fabric RVE (1/2 period shown).

6. Effective stiffness

The surfaces that bound the inclusions can now be used to compute the volume fraction of the inclusions to the entire RVE, as well as the g-integrals (Eq. (15)), FS^{P} (Eq. (11)), S^{P} (Eq. (14)), and A (Eq. (17)). Each of these expressions is evaluated for a given number of terms N [see Eq. (3)]. In addition, it is assumed that the direction of the fibers within each inclusion is parallel to the slope of the undulation. The inclusions are treated as unidirectional composites with average properties. Existing micromechanical models (Luciano and Barbero, 1994; Barbero and Luciano, 1995) are used to determine the material properties in terms of fiber and matrix properties within each inclusion, resulting in transversely isotropic material properties for each inclusion. The g-integral is evaluated for each inclusion according to the following expanded form

$$g_{\mathrm{Tf1}}(-\underline{\xi}) = \frac{1}{v_{\mathrm{Tf1}}} \int_{-a_2}^{a_2} \int_{-a_x}^{-a_g} \int_{\mathrm{bot}_{\mathrm{f1}}(x,y)}^{\mathrm{top}_{\mathrm{f1}}(x,y)} \exp\left(-\mathrm{i}\pi\left(\frac{n_1 x}{a_1} + \frac{n_2 y}{a_2} + \frac{n_3 z}{a_3}\right)\right) \mathrm{d}z\,\mathrm{d}x\,\mathrm{d}y \tag{39}$$

in which the terms $\mathrm{bot}_{\mathrm{f1}}(x,y)$ and $\mathrm{top}_{\mathrm{f1}}(x,y)$ are the surface functions that bound the inclusions and the x term has been expanded to show the indices n_1, n_2, and n_3. The volume of the inclusion, v_{Tf1}, is determined by simply evaluating Eq. (39) without the exponential term. The Fourier coefficient of S^{P} is simplified with the assumption that an isotropic matrix surrounds the inclusions. With this assumption, the local stiffness of the matrix is no longer a function of position, and the simplified term for FS^{P} is written as

$$FS^{\mathrm{P}}(\xi) = 2\mathrm{sym}\left(\bar{\xi} \otimes I^{(2)} \otimes \bar{\xi}\right) - \frac{1}{1-v}\bar{\xi} \otimes \bar{\xi} \otimes \bar{\xi} \otimes \bar{\xi} + \frac{1}{1-v}\bar{\xi} \otimes \bar{\xi} \otimes I^{(2)} \tag{40}$$

or in indicial notation

$$FS^{\mathrm{P}}_{ijkl}(\underline{\xi})_{\mathrm{iso}} = \frac{1}{2}\left[\bar{\xi}_j\left(\delta_{il}\bar{\xi}_k + \delta_{ik}\bar{\xi}_l\right) + \bar{\xi}_i\left(\delta_{jl}\bar{\xi}_k + \delta_{jk}\bar{\xi}_l\right)\right] - \frac{1}{1-v}\left(\bar{\xi}_i\bar{\xi}_j\bar{\xi}_k\bar{\xi}_l\right) + \bar{\xi}_i\bar{\xi}_j\delta_{kl} \tag{41}$$

in which the only material property remaining is the Poisson's ratio of the matrix and

$$\bar{\underline{\xi}} = \frac{\underline{\xi}}{|\underline{\xi}|}. \tag{42}$$

A Mathcad™ sub-routine is written to evaluate Eq. (41) in contracted notation, the result of which is a 6×6 matrix. From the evaluation of the g-integrals and FS^{P}, the periodic integral operator S^{P} can be determined according to Eq. (14) in which f_α is the mesoscale volume fraction of a given inclusion to the entire RVE, denoted as

$$f_\alpha = \frac{v_{\mathrm{Tf1}}}{v_{\mathrm{RVE}}}. \tag{43}$$

The final term to be evaluated in order to solve for the effective stiffness matrix is a combination of the previously evaluated terms, which is determined according to Eq. (17). From the steps outlined previously, the effective stiffness of the homogenized plain weave fabric RVE can be determined for a given value of N.

7. Results

The equations necessary for determining the effective stiffness matrix are written into a general Mathcad™ template, which can be modified for a plain weave fabric composite with any combination of fabric architecture dimensions and constituent materials. Using Section 5.2 to represent the fabric geometry, a Mathcad™ file is generated and the properties are calculated for the plain weave fabric architectures in (Ito and Chou, 1998; Scida et al., 1999; Kollegal and Sridharan, 2000b; Sheng and Hoa, 2001) and compared with experimental and/or existing model results. The results are listed in Tables 3–6. For the material

Table 3
Comparison of periodic microstructure vs. experimental results from (Ito and Chou, 1998) for an AS4/vinylester plain weave fabric composite ($N = 5$)

	Effective material properties	
	Periodic microstructure	Ito and Chou (experimental)
E_x	44.602 GPa	~43.5 GPa
E_y	43.714 GPa	–
E_z	9.997 GPa	–
G_{yz}	2.909 GPa	–
G_{xz}	2.887 GPa	–
G_{xy}	3.608 GPa	–
v_{yz}	0.411	–
v_{xz}	0.404	–
v_{xy}	0.062	–

Table 4
Comparison of periodic microstructure vs. the experimental results from (Scida et al., 1999) for an E-glass/vinylester plain weave fabric composite ($N = 5$)

	Effective material properties	
	Periodic microstructure	Scida et al. (experimental)
E_x (GPa)	24.9	24.8 ± 1.1
E_y (GPa)	24.9	24.8 ± 1.1
E_z (GPa)	10.4	8.5 ± 2.6
G_{yz} (GPa)	2.91	4.2 ± 0.7
G_{xz} (GPa)	2.91	4.2 ± 0.7
G_{xy} (GPa)	4.38	6.5 ± 0.8
v_{yz}	0.345	0.28 ± 0.07
v_{xz}	0.345	0.28 ± 0.07
v_{xy}	0.130	0.1 ± 0.01

Table 5
Comparison of periodic microstructure vs. experimental results from (Kollegal and Sridharan, 2000b) for an E-glass/epoxy plain weave fabric composite ($N = 5$)

	Effective material properties	
	Periodic microstructure	Kollegal and Sridharan (experimental)
E_x	18.902 (GPa)	19.29 (GPa)
E_y	18.902 (GPa)	–
E_z	8.735 (GPa)	–
G_{yz}	2.567 (GPa)	–
G_{xz}	2.567 (GPa)	–
G_{xy}	3.065 (GPa)	3.18 (GPa)
v_{yz}	0.437	–
v_{xz}	0.437	–
v_{xy}	0.129	0.2

from (Ito and Chou, 1998), the fiber volume fraction of each tow (Table 1) is calculated from the volume fraction of the tows in the RVE V_{inc} and the overall fiber volume fraction $V_{\text{f,o}}$ according to

Table 6
Comparison of periodic microstructure vs. experimental results from (Sheng and Hoa, 2001) for a T300/epoxy plain weave fabric composite ($N = 5$)

	Effective material properties	
	Periodic Microstructure	Sheng and Van Hoa (model)
E_x (GPa)	50.667	58.9
E_y(GPa)	49.778	52.1
E_z (GPa)	10.802	11.2
G_{yz} (GPa)	2.971	4.01
G_{xz} (GPa)	3.003	3.87
G_{xy} (GPa)	4.028	3.71
v_{yz}	0.391	0.460
v_{xz}	0.384	0.442
v_{xy}	0.063	0.048

$$V_{\mathrm{f,tow}} = \frac{V_{\mathrm{f,o}}}{V_{\mathrm{inc}}} \tag{44}$$

For the idealized geometry, periodic microstructure predictions in Tables 3–6 are in excellent agreement with the available experimental values. Modification of the Mathcad™ template for each material system consisted of merely changing the respective RVE dimensions and material properties for each case. The comprehensiveness of the model is especially seen in the comparison of predictions with experimental data of Scida et al. in (1999). The model predicts moduli values that are within or very near the published standard deviation. What is even more significant is the ability of the model to capture the interlaminar properties E_z, G_{yz}, and G_{xz}.

Fabric-reinforced composite properties predicted using the measured CERL geometry are shown in Table 7 and compared to those predicted using the idealized architecture. The idealized geometry is constructed using the outer dimensions of the CERL RVE ($a_1, a_2, a_3, a_{g1}, a_{g2}$ in Fig. 2). The inclusions are assumed to be AS4/vinylester for both geometries. The fiber volume fraction for the CERL geometry is calculated by Eq. (44) with V_{inc} calculated on the idealized geometry (based on the outer CERL dimensions) and using the published $V_{\mathrm{f,o}}$ for AS4-D Carbon/vinylester found (Table 1).

The comparison between the CERL geometry and the idealized geometry (Table 7) reveals the sensitivity of the periodic microstructure model to the geometry of the inclusions, specifically RVE dimensions and tow crimp. For the AS4/vinylester analysis using the CERL architecture, the tow crimp in the x-direction is significantly less than in the y-direction, resulting in an increase in the longitudinal modulus, E_x. Some of this effect is captured by the idealized model due variations in a_1 and a_2, but the effects of variations in tow

Table 7
Comparison of CERL and Ito and Chou fabric architectures for AS4/vinylester model results ($N = 5$)

	Effective material properties	
	CERL architecture	Idealized architecture
E_x (GPa)	40.654	41.106
E_y (GPa)	28.398	41.107
E_z (GPa)	7.901	9.807
G_{yz} (GPa)	2.251	3.077
G_{xz} (GPa)	2.201	3.077
G_{xy} (GPa)	3.054	3.574
v_{yz}	0.454	0.437
v_{xz}	0.431	0.437
v_{xy}	0.082	0.059

crimp between individual tows or weave directions is lost in the idealized geometry. It is shown in Table 7 that variations in tow crimp and fiber/matrix bundle diameter has a profound impact on the in-plane elastic moduli, E_x and E_y. There is a 35 percent difference between E_x and E_y when actual photomicrograph data are used, whereas no difference is seen between E_x and E_y when the idealized geometry is used, even though the dimensions of the RVE (a_1, a_2) are correctly represented (Table 3).

8. Conclusions

Based on the comparisons with experimental data for a variety of independent material systems, periodic microstructure is shown to predict well the complete set of effective orthotropic material properties for a plain weave fabric composite. Using periodic microstructure micromechanics, the rigorous mathematical framework of (Nemat-Nasser and Hori, 1993) is extended to predict the effects of multiple inclusions at the mesoscale for woven fabric composite materials using real and idealized geometric representations of the fabric RVE. The effective stiffness matrix (Eq. (16)) is modified to capture the interactive effects caused by multiple inclusions and a systematic approach is developed in Section 5 to characterize the inclusions in terms of three-dimensional surface functions. The necessary calculations are performed using Mathcad™, a commercially available mathematics software package. Three-dimensional mapping using photomicrograph data and idealized equations for a variety of plain weave composite data is used to develop sets of surface functions that represent the bounds of the warp and fill inclusions, as seen in Fig. 2. Using the periodic microstructure model to compare calculations performed with both geometries, it is seen from the results that the model is able to capture the interlaminar properties for a woven fabric composite, and that the in-plane moduli are sensitive to both tow crimp and RVE dimensions. The CERL geometry, due to uneven RVE dimensions and RVE face mismatch observed from photomicrograph data and captured by the curve fitting, is more sensitive to these effects than the idealized geometry. It is shown in Table 7 that the mismatch of the RVE can vary the longitudinal moduli of the fabric by 35%. The strength of the idealized geometry used in conjunction with Mathcad™ is that a wide variety of plain weave fabric architectures and materials systems can be easily solved from simple measurements of the RVE dimension and knowledge of the volume fraction of reinforcement fiber. From comparisons with experimental data on a variety of fabric geometries and material combinations, the model can easily and effectively predict the linear elastic material properties of plain weave fabric composites. This procedure has applications that extend beyond effective material property prediction of fabric-reinforced composites. Because of the generality of the derivation process, this technique could be applied to any periodically heterogeneous system, provided that the bounds of the heterogeneity can be quantified by surface functions.

References

Aboudi, J., 1991. Mechanics of Composite Materials: A Unified Micromechanical Approach. Elsevier Science, Netherlands.

Aitharaju, V.R., Averill, R.C., 1999. Three-dimensional properties of woven-fabric composites. Composites Science and Technology (59), 1901–1911.

Barbero, E.J., Luciano, R., 1995. Micromechanical formulas for the relaxation tensor of linear viscoelastic composites with transversely isotropic fibers. International Journal of Solids and Structures 32 (13), 1859–1872.

Blackketter, D.M., Walrath, D.E., Hansen, A.C., 1993. Modeling damage in a plain weave fabric-reinforced composite material. Journal of Composites Technology and Research 15 (2), 136–142.

Damiani, T.M., 2003. Mesomechanics of fabric reinforced composites. Ph.D. Dissertation, West Virginia University.

Dasgupta, A., Bhandarkar, S.M., 1994. Effective thermomechanical behavior of plain-weave fabric-reinforced composites using homogenization theory. Journal of Engineering Materials and Technology 116, 99–105.

Dasgupta, A., Agarwal, R.K., Bhandarkar, S.M., 1996. Three-dimensional modeling of woven-fabric composites for effective thermo-mechanical and thermal properties. Composites Science and Technology (56), 209–223.

Hahn, H.T., Pandey, R., 1994. A micromechanics model for thermoelastic properties of plain weave fabric composites. Journal of Engineering Materials and Technology 116, 517–523.

Ishikawa, T., Chou, T.W., 1982. Stiffness and strength behaviour of woven fabric composites. Journal of Materials Science (17), 3211–3220.

Ito, M., Chou, T.W., 1997. Elastic moduli and stress field of plain-weave composites under tensile loading. Composites Science and Technology (57), 787–800.

Ito, M., Chou, T.W., 1998. An analytical and experimental study of strength and failure behavior of plain weave composites. Journal of Composite Materials 32 (1), 2–30.

Kollegal, M.G., Sridharan, S., 1998. Compressive behavior of plain weave lamina. Journal of Composite Materials 32 (15), 1334–1355.

Kollegal, M.G., Sridharan, S., 2000a. Strength prediction of plain woven fabrics. Journal of Composite Materials 34 (3), 240–257.

Kollegal, M.G., Sridharan, S., 2000b. A simplified model for plain woven fabrics. Journal of Composite Materials 34 (20), 1756–1786.

Kuhn, J.L., Charalambides, P.G., 1998a. Elastic response of porous matrix plain weave fabric composites. Part I: modeling. Journal of Composite Materials 32 (16), 1426–1471.

Kuhn, J.L., Charalambides, P.G., 1998b. Elastic response of porous matrix plain weave fabric composites. Part II: results. Journal of Composite Materials 32 (16), 1472–1507.

Kuhn, J.L., Charalambides, P.G., 1999. Modeling of plain weave fabric composite geometry. Journal of Composite Materials 33 (3), 188–220.

Luciano, R., Barbero, E.J., 1994. Formulas for the stiffness of composites with periodic microstructure. International Journal of Solids and Structures (31), 2933–2944.

Mori, T., Tanaka, K., 1973. Average stress in matrix and average elastic energy of materials with misfitting inclusions. Acta Metallurgy 21, 571–574.

Naik, N.K., Ganesh, V.K., 1996. Failure behaviour of plain weave fabric laminates under on-axis uniaxial tensile loading II—analytical predictions. Journal of Composite Materials 30 (6), 1779–1821.

Nemat-Nasser, S., Hori, M., 1993. Micromechanics: Overall Properties of Heterogeneous Materials. Elsevier Science, Amsterdam.

Nemat-Nasser, S., Yu, N., Hori, M., 1993. Bounds and estimates of overall moduli of composites with periodic microstructure. Mechanics of Materials 15, 163–181.

Scida, D., Aboura, Z., Benzeggagh, M.L., Bocherens, E., 1999. A micromechanics model for 3D elasticity and failure of woven-fibre composite materials. Composites Science and Technology (59), 505–517.

Sheng, S.Z., Hoa, S.V., 2001. Three dimensional micro-mechancial modeling of woven fabric composites. Journal of Composite Materials 35 (19), 1701–1729.

Vandeurzen, Ph., Ivens, J., Verpoest, I., 1996a. A three-dimensional micromechanical analysis of woven-fabric composites: I. Geometric analysis. Composites Science and Technology (56), 1303–1315.

Vandeurzen, Ph., Ivens, J., Verpoest, I., 1996b. A three-dimensional micromechanical analysis of woven-fabric composites: II. Elastic analysis. Composites Science and Technology (56), 1317–1327.

Weng, G.J., 1984. Some elastic properties of reinforced solids with special reference to isotropic ones containing spherical inclusions. International Journal of Engineering Science 22, 845–856.

Zhang, Y.C., Harding, J., 1990. A numerical micromechanics analysis of the mechanical properties of a plain weave composite. Composites and Structures 36 (5), 839–844.

Zhong, S., Van Hoa, S., 2001. Three dimensional micro-mechanical modeling of woven fabric composites. Journal of Composite Materials 35 (19), 1701–1729.